Laser and Particle Beams (2017), *35*, 234–240.

doi:10.1017/S0263034617000106

Generating high-yield positrons and relativistic collisionless shocks by 10 PW laser

J. JIAO,[1,2] B. ZHANG,[1,2] J. YU,[3] Z. ZHANG,[1,2] Y. YAN,[1,2] S. HE,[1,2] Z. DENG,[1,2] J. TENG,[1,2] W. HONG,[1,2] AND Y. GU[1,2,4,5]

[1]Science and Technology on Plasma Physics Laboratory, Research Center of Laser Fusion, Mianyang, Sichuan, China
[2]Academy of Engineering Physics, Mianyang, Sichuan, China
[3]Blackett Laboratory, The John Adams Institute for Accelerator Science, Imperial College, London, UK
[4]IFSA Collaborative innovation center, Shanghai Jiao Tong University, Shanghai, China
[5]HEDPS, Center for Applied Physics and Technology, Peking University, Beijing, China

(RECEIVED 19 September 2016; ACCEPTED 23 January 2017)

Abstract

Relativistic collisionless shock charged particle acceleration is considered as a possible origin of high-energy cosmic rays. However, it is hard to explore the nature of relativistic collisionless shock due to its low occurring frequency and remote detecting distance. Recently, there are some works attempt to solve this problem by generating relativistic collisionless shock in laboratory conditions. In laboratory, the scheme of generation of relativistic collisionless shock is that two electron–positron pair plasmas knock each other. However, in laboratory, the appropriate pair plasmas have been not generated. The 10 PW laser pulse maybe generates the pair plasmas that satisfy the formation condition of relativistic collisionless shock due to its ultrahigh intensity and energy. In this paper, we study the positron production by ultraintense laser high Z target interaction using numerical simulations, which consider quantum electrodynamics effect. The simulation results show that the forward positron beam up to 10^{13}/kJ can be generated by 10 PW laser pulse interacting with lead target. The estimation of relativistic collisionless shock formation shows that the positron yield satisfies formation condition and the positron divergence needs to be controlled. Our results indicate that the generation of relativistic collisionless shock by 10 PW laser facilities in laboratory is possible.

Keywords: Laser–plasma interaction; Positron production; Relativistic collisionless shock; 10 PW laser

1. INTRODUCTION

Positron beams generated by interaction of ultraintense laser with plasma have several advantages, such as high yield and short duration, which is propitious to produce dense relativistic positron–electron pair plasma. Such pair plasma is interesting to many fields of high-energy astrophysics, such as gamma ray bursts, active galactic nuclei and pulsar wind nebulae (Piran, 2005; Meszaros, 2006). A possible explanation for the origin of high-energy cosmic rays is that relativistic collisionless shock generated by collision of pair plasmas accelerates charged particles to very high energy by Fermi acceleration mechanism (Spitkovsky, 2008). Laser-driven relativistic positron–electron pair plasma supports opportunity to study the relativistic collisionless shock in laboratory conditions.

At present, there are mainly two approaches to generate relativistic positron–electron pair plasmas by laser in laboratory, the direct and the indirect approach. The direct positron-generation is to interact of ultraintense laser with high Z solid target directly, positrons are produced by Trident and Bethe–Heitler (B–H) process when hot electrons penetrate high Z target (Chen *et al.*, 2015*a*). The indirect method employed table-top laser to interact with a gas jet to accelerate energetic electrons, and positrons are then produced when these electrons impinging a secondary high Z target (Gahn *et al.*, 2000; Sarri *et al.*, 2015*a*). Considering high positron yield is necessary for demonstrably relativistic collisionless shocks in laboratory, Chen *et al.* (2015*a*) have performed several positron-generation experiments by the direct approach, found that positron yield increases with both laser energy and intensity. Typical 10 PW laser facilities, such as ELI or VULCAN (Hernandez-Gomez *et al.*, 2010), which will realize laser intensity above 10^{23} W/cm^2 are certainly better to demonstrate positron–electron plasma collisionless shocks. However, so far, there is no detailed study of the characteristics of positrons on 10 PW laser

Address correspondence and reprint requests to: E-mail: yqgu@caep.cn

facilities, and it is still unclear if the characteristics of positrons on 10 PW laser facilities would satisfy the formation condition of relativistic collisionless shock.

In this paper, the yield, energy spectrum and angular distribution of positrons generated via ultraintense laser high Z target interaction were investigated in full physical process by use of numerical simulation. Firstly, we use radiation hydrodynamics code to simulate the interactions of amplified spontaneous emission (ASE) before main laser pulse with the high Z target, which gives the preplasma electron density profile. Then we get the information of gamma rays and hot electrons ultraintense laser main pulse interacting with preplasma by particle-in-cell (PIC) code with quantum electrodynamics (QED) effect. Finally, we simulate the positrons generation by the gamma rays and hot electrons propagate in the high Z target with Monte Carlo code. The simulation results show that forward positron beam with yield up to 10^{13}/kJ can be produced using 30 fs ultraintense laser with its intensity 10^{22}–10^{23} W/cm^2. The theoretical analysis indicates that this yield of positron beam satisfies the formation condition of relativistic collisionless shock.

2. SIMULATION METHOD

Positron generation by interaction of ultraintense laser with solid target includes several physical processes with different temporal and spatial scales. In this study, the simulation of positrons generation has three steps: step 1, we use one-dimensional (1D) radiation hydrodynamics code Multi1D to simulate the process of ultraintense laser ASE interacting with the high Z target, in this step, preplasma electrons density profile around critical density surface is acquired (blue region in Fig. 1). Step 2, generation of gamma rays and hot electrons is simulated with 3D PIC code Epoch, which includes QED effect, in the interaction of ultraintense laser main pulse with the preplasma (purple region in Fig. 1). Step 3, we simulate the positrons generation using Monte Carlo code Fluka when the gamma rays and hot electrons impinge the high Z target (yellow region in Fig. 1).

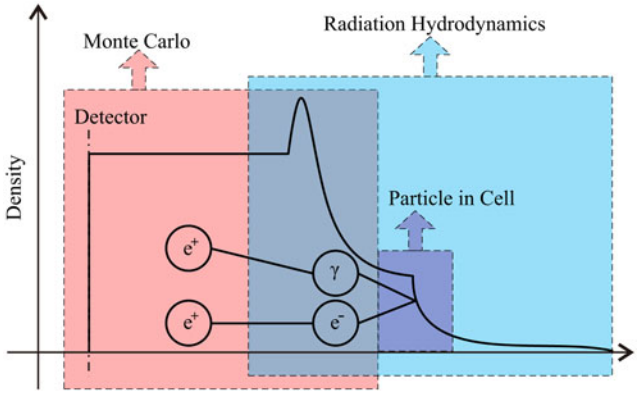

Fig. 1. Illustration of numerical simulation schemes.

When using PIC code to simulate the interaction of ultraintense laser pulse with solid target, one usually assume that the solid target preplasma has an exponential density profile with certain density scale length (Hanus *et al.*, 2014). However, when laser ASE has a high intensity, the preplasma density profile around the critical density surface could be different due to the laser light pressure. In order to acquire accurate preplasma density profile, which is important for hot electron generation, we use 1D radiation hydrodynamics code Multi1D (Ramis *et al.*, 1988) to simulate the interaction of ultraintense laser ASE with the high Z target.

Single-particle dynamics effect becomes very important when ultraintense laser main pulse reaches the plasma. Electrons acquire energy from the laser by collisionless absorption mechanisms. Furthermore, gamma photons, radiation by accelerated electrons would become prominent when laser intensity exceeds 10^{22}W/cm^2. The expression of parameter χ is $\chi = e\hbar/m_e^3c^4\sqrt{((\varepsilon\vec{E}/c)+\vec{p}\times\vec{H})^2-(\vec{p}\cdot\vec{E})^2}$. The peak value of χ can be estimated as $\chi \sim \gamma_0\, a_0\, (r_e/\lambda_0)(2\pi/\alpha)$, where $r_e = e^2/m_ec^2$ is the classic electron radius, $\alpha = e^2/\hbar c$ is the fine-structure constant. For the case in Section 3.2, a laser with $\lambda_0 = 1$ μm and $a_0 = 600$, and electron relativistic factor $\gamma_0 = 500$, we have $\chi \sim 0.75$. Thus, the QED effect becomes an important role and should be considered. In order to acquire velocities and energy information of gamma rays and hot electrons, we simulated the interaction of ultraintense laser pulse with solid target preplasma with 3D PIC code Epoch (Arber *et al.*, 2015). Epoch code which includes QED effects can simulate synchrotron emission of high-energy gamma rays generated when electrons oscillating in the laser field.

Positrons are created mainly through three processes: (a) The Trident process, where positrons are produced directly by energetic electrons interacting with Coulomb field of nucleus. (b) The B–H process, where positrons are generated indirectly via bremsstrahlung photons. (c) The multiphoton Breit–Wheeler process (B–W), $\gamma_h + n\gamma_l \rightarrow e^- + e^+$, where γ_h is gamma photon and γ_l is laser photon. Previous studies show that positron generation is dominated by B–H process in thick targets (Liang *et al.*, 1998) and by Trident process in thin target (less than tens micrometers) (Shen & Meyer-ter-Vehn, 2001). Considering the positron yield of B–W process is about 10^9/kJ under conditions similar to our study (Ridgers *et al.*, 2012), which is much less than the 10^{13}/kJ yield of B–H process. Thus in our simulations the positrons are mainly generated through B–H process.

3. RESULTS AND DISCUSSION

3.1. Preplasma density profile

We use Multi1D to simulate laser ASE interaction with Pb target. The laser wavelength is 1 μm, and we assume the laser contrast ratio is 10^{-9} ASE intensity is 5×10^{14} W/cm^2, which is a typical value in ultrashort and ultraintense

https://doi.org/10.1017/S0263034617000106 Published online by Cambridge University Press

laser facility. The ASE intensity grows linearly from $t = 0$ to 0.1 ns and keeps constant for 1.2 ns. The density and thickness of Pb target is 11.34 g/cc and 200 μm, respectively. The initial temperature of electron and ion is 0.03 eV (300 K). In our simulation, the laser lost 50% of its energy around the critical density surface and electron heat flux limit factor 0.05 was used.

Figure 2 is the electron density profile of fully ionized Pb plasma at 1.2 ns, it shows that density profile increases rapidly from 1 n_c to 40 n_c and then increases slowly. Around critical density surface, a part of laser energy is transferred to high-energy electrons by resonance absorption and inverse bremsstrahlung absorption. A shock is formed due to the high-energy electrons ablating solid target. The plasma between the shock and the critical density surface expands along the inverse laser propagation direction due to high-energy electron heating. When laser light pressure is high enough, the plasma expansion would be restrained; hence, a plasma density jump around the critical density surface is formed (Attwood *et al.*, 1978).

3.2. Photon and electron generation

We get the velocity and energy of gamma photons and hot electrons with 3D PIC code EPOCH. The laser peak intensity is 5×10^{23} W/cm^2, corresponding to a normalized laser vector potential $a_0 = 602$ and the laser electric field intensity profile is $a = a_0 \sin^2(\pi t/2\tau)\exp(-(r/r_0)^2)$, where $\tau = 30$ fs is the duration and $r_0 = 2\lambda_0$ (laser wavelength $\lambda_0 = 1$ μm) is the spot size. It is polarized along the *Y*-direction and propagates along the *X*–direction, and the total laser energy is about 706 J. The simulation box is $X \times Y \times Z = 30\ \mu m \times 16\ \mu m \times 16\ \mu m$, with a cell size of $dX \times dY \times dZ = 0.0\,6\ \mu m \times 0.064\ \mu m \times 0.064\ \mu m$. The fully ionized Pb plasma with electron density 40 n_c is initially located from $x = 5$ to 30 μm. The initial temperature of electron and Pb ion is 1 keV. The macroparticle number of electron and ion per cell is 20 and 10, respectively. The field- and particle boundary conditions at the left hand of the *X*-direction are absorptive, and the particle boundary in the *Y* and *Z*-directions and the right-hand of the *X*-direction are thermal, which means that the particles are re-injected into the box with a thermal velocity at the boundaries.

In this simulation, the motion of gamma photons is suspended right after generated. We get information of gamma photons that propagate along the *X*-positive direction, from the simulation box at simulation time 160 fs. The hot electrons come from two parts in this simulation. The first part is the electrons stay at the simulation box at 160 fs; the second part is the electrons pass through the diagnostic surfaces from $t = 0$ to 160 fs. The diagnostic surface is located at the left, right, up, down, front boundary of the simulation box along the *X*-positive direction, respectively. The electron will be recorded when it passes through the diagnostic surface from the box inner region to the boundaries.

Gamma photons and hot electrons with their energy beyond the positron generation threshold 1.022 MeV and propagate forward are selected. Information of these gamma photons and hot electrons generated from $t = 0$ to $t = 160$ fs are collected to simulate positron generation (in Fig. 3). We selected 160 fs because it is the time that laser energy is almost completely exhausted. To estimate the influence of QED effect, we carried out simulations both with and without considering QED effects. In the case of including QED effect, the spectra of gamma photon and hot electron

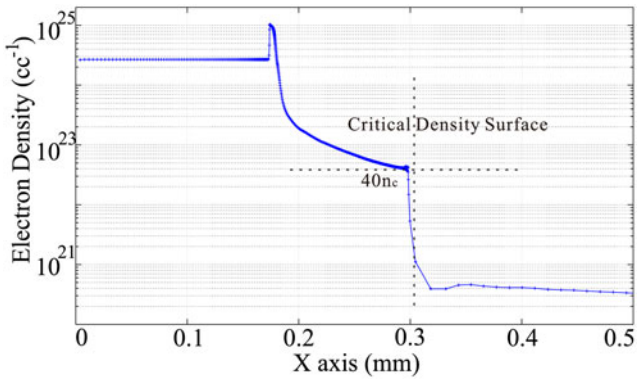

Fig. 2. Electron density profile of fully ionization Pb target at 1.2 ns.

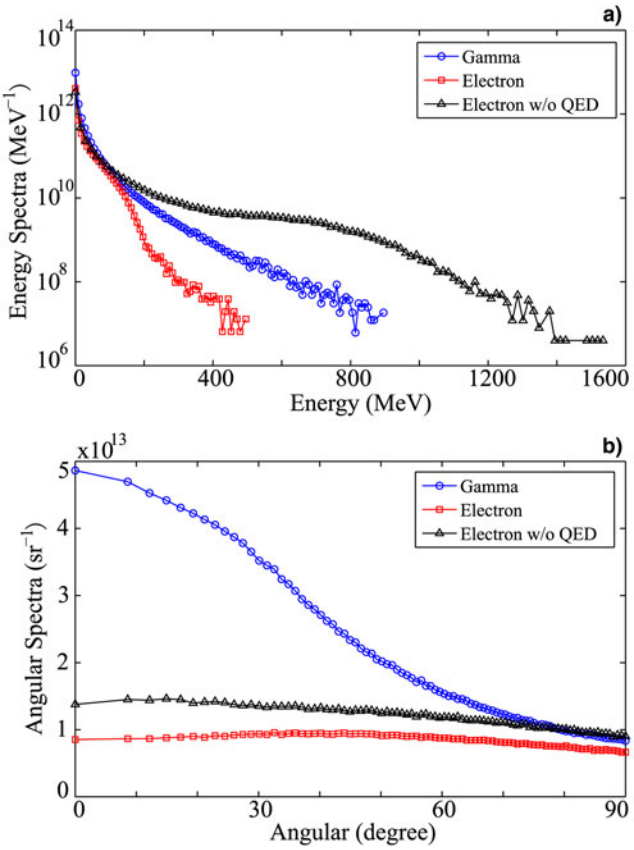

Fig. 3. Spectra and angular distribution of photons and electrons. (a) Spectra; (b) Angular distribution.

https://doi.org/10.1017/S0263034617000106 Published online by Cambridge University Press

show that the particles with energy up to several hundred MeV are generated (in Fig. 3a). The energy conversion efficiency from laser to gamma photons is 42% [This conversion efficiency is consistent with the result reported by Ji *et al.* (2014*b*) and Brady *et al.* (2014)] and is 20% for hot electrons. The angular distribution shows that hot electrons are approximately isotropically emitted, while gamma photons are emitted along the forward direction with a half-divergence angle of 0.7 rad (40°) (Fig. 3b). In comparison, without QED effect (the black line in Fig. 3), the number of the high-energy electrons is overestimated, which would lead to overestimate of positron number and cutoff energy. Thus, it is necessary to consider QED effect in PIC simulations of the interaction of 10 PW laser with plasmas. In addition, the energy conversion efficiency from laser to hot electrons is 63%, which is close to the energy conversion efficiency from laser to gamma photons and hot electrons in the QED effects included case. The angular distribution of hot electrons in this case is also approximately isotropic (in Fig. 3b).

In the simulation with QED effect, the electrons acquire energy from laser field by the $\mathbf{J}\times\mathbf{B}$ acceleration mechanism (Wilks *et al.*, 1992) because of the momentum profile of electrons in the *X*-direction includes periodic structure with $\lambda/2$ as shown in Figure 4d. The synchrotron emission of gamma photons will be generated when the high-energy electrons are oscillating in the laser field (in Fig. 4c) (Brady *et al.*, 2014), and this emission of photons exert a radiation reaction force on the oscillating electrons. The oscillating electrons will be trapped in the laser field when the radiation reaction force exceeds laser ponderomotive force (Ji *et al.*, 2014*a*), and continuously transfer laser energy to gamma photons. The radiation reaction effect significantly reduces the electrons oscillation amplitude; this can be found by comparing the electron densities in Figures 4a and 4b; therefore reduces the number of high-energy electrons and photons shown as in Figure 3a.

Compared with the interaction of laser with lower intensity $10^{18}-10^{21}$ W/cm^2 with plasmas, there are two advantages for positron production in the case of higher laser intensity around 10^{23} W/cm^2. (i) Higher photon and electron energy: this improves the positrons yields because the positron generation cross-section increases with the energy of photon and electron. (ii) Higher laser energy conversion efficiency: when lower intensity laser interacts with the preplasma, hot electrons (gamma photons are rarefied and ignored) are generated by collisionless absorption mechanisms, such as resonance absorption (Kruer, 1988), relativistic $\mathbf{J}\times\mathbf{B}$ heating (Wilks *et al.*, 1992) and direct laser acceleration (Pukhov *et al.*, 1999). In these mechanisms, a significant part of laser energy is reflected near the critical density surface. This leads to an energy conversion efficiency to forward hot electrons of about 30% in general (Gibbon, 2005). In the case of higher intensity laser, the laser energy is consumed by the plasma rapidly via accelerating electrons and emitting photons and almost have no laser reflection. The laser energy conversion efficiency to forward electrons and photons can reach 60%, much higher than the case of lower laser intensity obviously.

3.3. Positron characters from Pb converter

The positron production is simulated with Monte Carlo code Fluka (Battistoni *et al.*, 2007), gamma photons and hot electrons impinging a columned Pb target with radius 1 cm, whose thickness ranges from 0.05 to 1.5 cm. Positrons are recorded by the detector on the rear surface of the Pb target (in Fig. 1). Figure 5 shows the characteristics of positrons generated by interacting ultraintense laser with intensity of 5×10^{23} W/cm^2 with different Pb targets. These characteristics

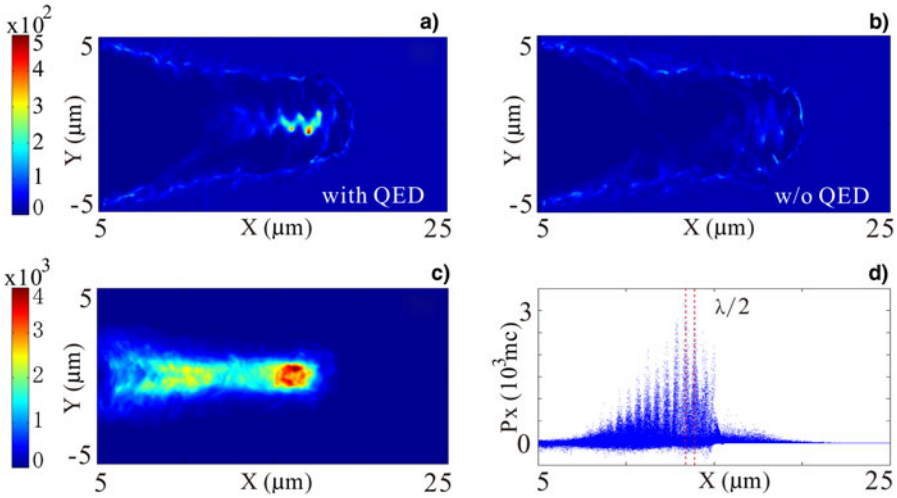

Fig. 4. Electron densities in the *X*–*Y* plane at $t = 100$ fs with QED effect (a) and w/o QED effect (b), respectively. (c) Gamma photon density profile at 100 fs. (d) Phase space distribution of electrons in frame (a). The unit for density is the critical density n_c.

https://doi.org/10.1017/S0263034617000106 Published online by Cambridge University Press

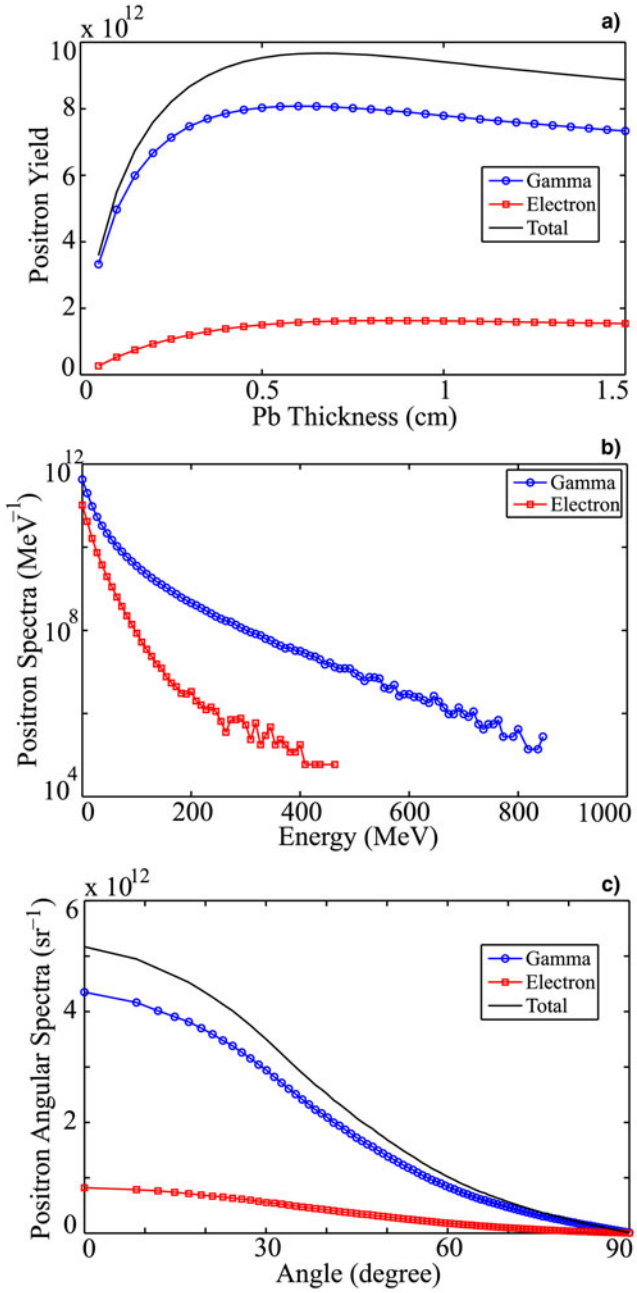

Fig. 5. Comparison of positrons generated directly by photons and electrons in the Pb target. (a) Positrons yield versus Pb target thickness. (b) Positron energy spectrum. (c) Positron angular distribution.

will be used when we estimate the positron yield of relativistic collisionless shock formation in Section 3.5.

Positron yield: We obtain the maximum positrons yield of 1.38×10^{13}/kJ at the optimal Pb target thickness of 6 mm (in Fig. 5a). This positron yield is one to two orders higher than that in the works using lasers with intensity below 10^{21} W/cm^2 (Myatt *et al*., 2009; Chen *et al*., 2015*a*). It is important to note that we do not consider the effect of hot electron refluxing that is considered by Chen *et al*. (2015*a*), and can further improve positron yield.

Optimal thickness: The optimal target thickness is determined by the radiation length ($L_{\rm rad}$) of the material, which can be seen as the average distance needed to perform one step of the cascade (either photon creation by bremsstrahlung or generation of an electron–positron pair). The radiation length is approximately given by $L_{\rm rad} = 1/[4\alpha(Z\alpha)^2 n\lambda_{\rm C}^2 L_0]$, where n is the number of atoms per unit volume, $\alpha \approx 1/137$ is the fine structure constant, $\lambda_{\rm C} = 3.9 \times 10^{-11}$ cm is the Compton wavelength and $L_0 = \log(183Z^{-1/3}) - f(Z\alpha)$, with $f(x) = \sum_{a=1}^{\infty} x^2/a(a^2 + x^2)$. Put corresponding parameters in, we can obtain the radiation lengths of Pb is 5.6 mm (Sarri *et al*., 2015*b*), which is consistent to the optimal target thickness.

Positron Temperature and Divergence: The positrons temperature is 78 MeV obtained from positron spectra as shown in Fig. 5b. Since the positrons are emitted along the forward direction with an large half angle of 0.7 rad (40°), the pair plasma density declines rapidly as the jet propagate away from the target, which is unpropitious for the formation of relativistic collisionless shock. Certainly, there are methods to collimate electron–positron jets, such as intense magnetic field along with target normal direction suggested by Chen *et al*. (2015*b*), or the concave rear surface target suggested by Wilks *et al*. (2001) to collimate proton beams, which can also collimate positron beams.

3.4. Positron yield and laser intensity

In a real ultraintense laser plasma experiment, the intensity of 10 PW laser facility might be actually below 5×10^{23} W/cm^2. Thus, it is necessary to study the dependence of positron yield on laser intensity from 5×10^{22} to 5×10^{23} W/cm^2. This dependence is given in Figure 6a. It can be found in Figure 6a that the positron yield per kJ through gamma photons increases with the laser intensity and that through electrons decreases with laser intensity. However, the total positron yield per kJ only has a weak dependence on laser intensity in this range.

There are two main reasons for the weak dependence: (i) the correspondingly relativistic plasma critical density $\gamma n_{\rm c}$ ($\gamma = \sqrt{1 + a_0^2/2}$) is ranging from 134 $n_{\rm c}$ to 426 $n_{\rm c}$ when the laser intensity changes from 5×10^{22} to 5×10^{23} W/cm^2, which is far beyond the preplasma density, which correspondingly changes from 10 $n_{\rm c}$ to 40 $n_{\rm c}$ calculated by Multi1D code and shown in Figure 6b. Thus, the laser pulse can penetrate the preplasma with almost no reflection due to relativistic transparency effect and generate hot electrons, gamma photons, and energetic ions. The PIC numerical simulations show that the forward hot electrons and gamma photons with energy beyond 1.022 MeV carry about 60% of laser energy, and this number is approximately independent of the laser intensity. (ii) The variety of positron production cross-section is slow when the energy of hot electrons and gamma photons reaches several tens MeV. These

https://doi.org/10.1017/S0263034617000106 Published online by Cambridge University Press

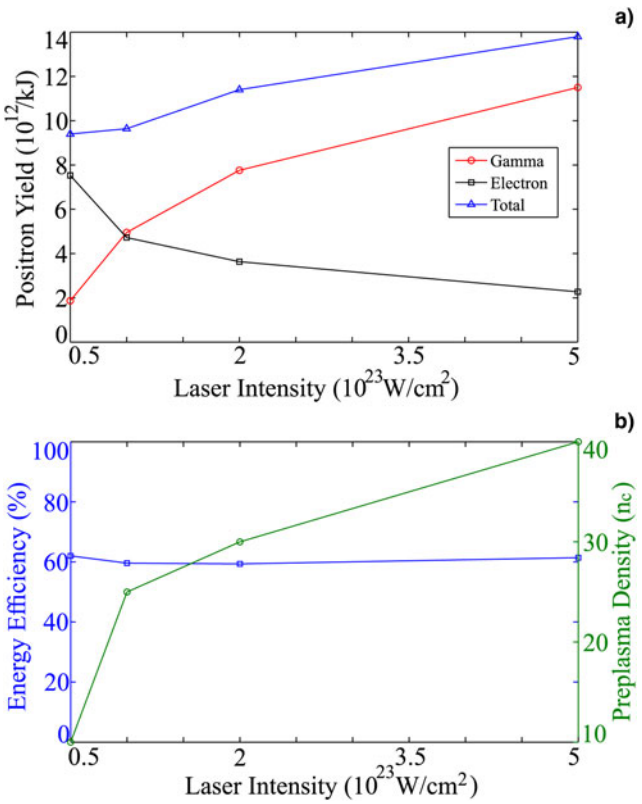

Fig. 6. Dependence of positron yield and preplasma density on laser intensity.

two factors lead to total positron yield per kJ have little difference with various laser intensity.

3.5. Relativistic collisionless shock formation

To generate relativistic collisionless shocks using two positron–electron counter-stream plasmas, the duration (τ) and radius (R) of pair plasmas being larger than temporal and spatial scale of the Weibel instability must be guaranteed (Chen *et al.*, 2015*a*). Namely, $\tau > 1/\Gamma$ and $R > c/\omega_p$, where $\Gamma = \sqrt{2}(v_0/c)\omega_p$ is the growth rate of Weibel instability for two counter-stream symmetric pair plasmas, where v_0, γ_0, and n_0 are the velocity, Lorentz factor, and density of pair plasmas, respectively.

Firstly, we estimate the positron yield to see whether relativistic collisionless shock formation is possible in the interaction of a laser pulse of 5×10^{22} W/cm^2 with 6 mm thickness Pb target by the simulation case. The hot electrons, which produce positrons penetrate the Pb target with velocities ranging from 0.943c to ~c (the corresponding electrons energy exceed 1.022 MeV). The duration of hot electron beam will reach ~1 ps at the position of radiation length (6 mm) in Pb target. The majority of positrons are generated at the position of radiation length; thus, the duration of positron beam is ~1 ps, in addition, $v_0 \sim c$ and $\gamma_0 \sim 100$. Using these parameters and the temporal and spatial conditions of relativistic collisionless shock formation, one can find that the density and radius of positron beams must satisfy $n_0 > 1.5 \times 10^{16}$/cc and $R > 0.4$ mm. The positron yield required for relativistic collisionless shock formation is $N = \pi R^2 c\tau n_0 > 2.2 \times 10^{12}$. In our simulations, the positron yield 10^{13}/kJ can be achieved with 10 PW laser. Then a 10 PW laser pulse, which usually contains energy up to several hundred or even a thousand Joule can produce more than 2.2×10^{12} positrons. This indicates that the positrons yield satisfies the formation condition of relativistic collisionless shock.

Secondly, we estimate the positron density to see if relativistic collisionless shock formation is possible. The positron beam radius R is ~4 mm when beam transport radiation length (6 mm) with half-angle of 0.7 rad. We assume that the positron number is 10^{13}, the positron density $\sim 7 \times 10^{14}$/cc near the target rear surface is then obtained. This positron beam density is too lower to generate relativistic collisionless shock (1.5×10^{16}/cc). However, we could use some methods, such as additional intense magnetic field and special structure target, to reduce the positron beam divergence to ~0.1 rad, and then to satisfy the formation condition of relativistic collisionless shock.

4. CONCLUSION

In summary, positron generation in ultraintense laser with interaction high Z target was investigated with radiation hydrodynamics, PIC and Monte Carlo numerical simulation codes. Our simulation results show that forward positron beam with the yield up to 10^{13}/kJ can be produced with ultraintense laser with duration 30 fs and intensity $10^{22} - 10^{23}$ W/cm^2. Such positron–electron beam is propitious to form positron–electron pair plasma and provide the opportunity to study relativistic collisionless shock in laboratory.

ACKNOWLEDGEMENTS

The author J. Jiao wishes to thank Dr. B. Yang for the help of Fluka code simulation. This work was supported by the Science Challenge Program and the Development Foundation of China Academy of Engineering Physics (grant no. 2013A0103003).

REFERENCES

Arber, T.D., Bennett, K., Brady, C.S., Lawrence-Douglas, A., Ramsay, M.G., Sircombe, N.J., Gillies, P., Evans, R.G., Schmitz, H., Bell, A.R. & Ridgers, C.P. (2015). Contemporary particle-in-cell approach to laser-plasma modelling. *Plasma Phys. Control. Fusion* **57**, 113001.

Attwood, D.T., Sweeney, D.W., Auerbach, J.M. & Lee, P.H.Y. (1978). Interferometric confirmation of radiation–pressure effects in laser–plasma interactions. *Phys. Rev. Lett.* **40**, 184.

Battistoni, G., Muraro, S., Sala, P.R., Cerutti, F., Ferrari, A., Roesler, S., Fasso, A. & Ranft, J. (2007). The FLUKA code: Description and bench-marking. AIP Conf. Proc. **896**, 31–49.

Brady, C.S., Ridgers, C.P., Arber, T.D. & Bell, A.R. (2014). Synchrotron radiation, pair production, and longitudinal electron

https://doi.org/10.1017/S0263034617000106 Published online by Cambridge University Press

motion during 10–100 PW laser solid interactions. *Phys. Plasmas* **21**, 033108.

Chen, H., Fuiza, F., Link, A., Hazi, A., Hill, M., Hoarty, D., James, S., Kerr, S., Meyerhofer, D.D., Myatt, J., Sentoku, Y. & Williams, G.J. (2015*a*). Scaling the yield of laser-driven electron–positron jets to laboratory astrophysical applications. *Phys. Rev. Lett.* **114**, 215001.

Chen, H., Link, A., Sentoku, Y., Audebert, P., Fuiza, F., Hazi, A., Heeter, R.F., Hill, M., Hobbs, L., Kemp, A.J., Kemp, G.E., Kerr, S., Meyerhofer, D.D., Myatt, J., Nagel, S.R., Park, J., Tommasini, R. & Williams, G.J. (2015*b*). The scaling of electron and positron generation in intense laser–solid interactions. *Phys. Plasmas* **22**, 056705.

Gahn, C., Tsakiris, G.D., Pretzler, G., Witte, K.J., Delfin, C., Wahlstrom, C.G. & Habs, D. (2000). Generating positrons with femtosecond-laser pulses. *Appl. Phys. Lett.* **77**, 2662–2664.

Gibbon, P. (2005). *Short Pulse Laser Interactions with Matter*. London: Imperial College Press.

Hernandez-Gomez, C., Blake, S.P., Chekhlov, O., Clarke, R.J., Dunne, A.M., Galimberti, M., Hancock, S., Heathcote, R., Holligan, P., Lyachev, A., Matousek, P., Musgrave, I.O., Neely, D., Norreys, P.A., Ross, I., Tang, Y., Winstone, T.B., Wyborn, B.E. & Collier, J. (2010). The Vulcan 10 PW project. *J. Phys.: Conf. Ser.* **244**, 032006.

Hanus, V., Drska, L., D'Humieres, E. & Tikhonchuk, V. (2014). Numerical study of positron production with short-pulse high-intensity lasers. *Laser Part. Beams* **32**, 171–176.

Ji, L.L., Pukhov, A., Kostyukov, I.Yu., Shen, B.F. & Akli, K. (2014*a*). Radiation-reaction trapping of electrons in extreme laser fields. *Phys. Rev. Lett.* **112**, 145003.

Ji, L.L., Pukhov, A., Nerush, E.N., Kostyukov, I.Yu., Shen, B.F. & Akli, K. (2014*b*). Energy partition, γ γ-ray emission, and radiation reaction in the near-quantum electrodynamical regime of laser–plasma interaction. *Phys. Plasmas* **21**, 023109.

Kruer, W.L. (1988). *The Physics of Laser Plasma Interactions*. New York: Addison-Wesley.

Liang, E.P., Wilks, S.C. & Tabak, M. (1998). Pair production by ultraintense lasers. *Phys. Rev. Lett.* **81**, 4887.

Meszaros, P. (2006). *Gamma-ray bursts*. *Rep. Prog. Phys.* **69**, 2259.

Myatt, J., Delettrez, J.A., Maximov, A.V., Meyerhofer, D.D., Short, R.W., Stoeckl, C. & Storm, M. (2009). Optimizing electron–positron pair production on kilojoule-class high-intensity lasers for the purpose of pair-plasma creation. *Phys. Rev. E* **79**, 066409.

Piran, T. (2005). The physics of gamma-ray bursts. *Rev. Mod. Phys.* **76**, 1143.

Pukhov, A., Sheng, Z.M. & Meyer-ter-Vehn, J. (1999). Particle acceleration in relativistic laser channels. *Phys. Plasmas* **6**, 2847–2854.

Ramis, R., Schmalz, R. & Meyer-ter-Vehn, J. (1988). MULTI – a computer code for one-dimensional multigroup radiation hydrodynamics. *Comput. Phys. Commun.* **49**, 475–505.

Ridgers, C.P., Brady, C.S., Duclous, R., Kirk, J.G., Bennett, K., Arber, T.D., Robinson, A.P.L. & Bell, A.R. (2012). Dense electron-positron plasmas and ultraintense γ-rays from laser-irradiated solids. *Phys. Rev. Lett.* **108**, 165006.

Sarri, G., Dieckmann, M.E., Kourakis, I., Di Piazza, A., Reville, B., Keitel, C.H. & Zepf, M. (2015*a*). Overview of laser-driven generation of electron-positron beams. *J. Plasma Phys.* **81**, 455810401.

Sarri, G., Poder, K., Cole, J.M., Schumaker, W., Di Piazza, A., Reville, B., Dzelzainis, T., Doria, D. , Gizzi, L.A., Grittani, G., Kar, S., Keitel, C.H., Krushelnick, K., Kuschel, S., Mangles, S.P.D., Najmudin, Z., Shukla, N., Silva, L.O., Symes, D., Thomas, A.G.R., Vargas, M., Vieira, J. & Zepf, M. (2015*b*). Generation of neutral and high-density electron–positron pair plasmas in the laboratory. *Nat. Commun.* **6**, 6747.

Shen, B. & Meyer-ter-Vehn, J. (2001). Pair and γ-photon production from a thin foil confined by two laser pulse. *Phys. Rev. E* **65**, 016405.

Spitkovsky, A. (2008). Particle acceleration in relativistic collisionless shocks: fermi process at last? *Astrophys. J.* **682**, L5.

Wilks, S.C., Kruer, W.L., Tabak, M. & Langdon, A.B. (1992). Absorption of ultra-intense laser pulse. *Phys. Rev. Lett.* **69**, 1383.

Wilks, S.C., Langdon, A.B., Cowan, T.E., Roth, M., Singh, M., Hatchett, S., Key, M.H., Pennington, D., MacKinnon, A. & Snavely, R.A. (2001). Energetic proton generation in ultra-intense laser–solid interactions. *Phys. Plasmas* **8**, 542–549.

https://doi.org/10.1017/S0263034617000106 Published online by Cambridge University Press